Organic Electronics 13 (2012) 820–825

Contents lists available at SciVerse ScienceDirect

Organic Electronics

journal homepage: www.elsevier.com/locate/orgel

Highly enhanced electron injection in organic light-emitting diodes with an n-type semiconducting MnO_2 layer

Hyunbok Lee [a], Jeihyun Lee [a], Pyungeun Jeon [a], Kwangho Jeong [a], Yeonjin Yi [a,*], Tae Gun Kim [b,c], Jeong Won Kim [b,c], Jin Woo Lee [d]

[a] Institute of Physics and Applied Physics, Yonsei University, 50 Yonsei-ro, Seodaemoon-Gu, Seoul 120-749, Republic of Korea
[b] Korea Research Institute of Standards and Science, 267 Gajeong-ro, Daejeon 305-340, Republic of Korea
[c] University of Science and Technology, 217 Gajeong-ro, Daejeon 305-350, Republic of Korea
[d] LG Innotek, 379, Gasoo-Dong, Osan-City, Gyeonggi-Do 447-705, Republic of Korea

ARTICLE INFO

Article history:
Received 15 October 2011
Received in revised form 14 January 2012
Accepted 15 January 2012
Available online 11 February 2012

Keywords:
OLED
Electron injection layer
MnO_2
UPS
XPS
Electronic structure

ABSTRACT

Highly enhanced electron injection is demonstrated with a thin manganese dioxide (MnO_2) electron injection layer (EIL) in Alq_3-based organic light-emitting diodes. Insertion of the MnO_2 EIL between the Al cathode and Alq_3 results in highly improved device characteristics. *In situ* photoelectron spectroscopy shows remarkable reduction of the electron injection barrier without significant chemical reactions between Alq_3 and MnO_2, which could induce Alq_3 destruction. The reduction of the electron injection barrier is due to the n-type doping effect, and the lack of strong interfacial reaction is advantageous with regards to more efficient electron injection than a conventional LiF EIL. These properties render the MnO_2, a potential EIL.

1. Introduction

Organic light-emitting diodes (OLEDs) have been remarkably attractive for the last two decades due to their unique advantages, such as simple fabrication processes, wide viewing angles, light weight, and mechanical flexibility [1]. However, high charge-injection barrier from the electrode to organic semiconducting materials is one of the inveterate obstacles to design highly efficient OLEDs. Lowering the electron injection barrier in OLEDs especially is a prerequisite to balancing electrons with holes within an emission layer to maximize light emission because most organic semiconducting materials have lower electron mobility than that of hole. It has been reported that the insertion of an appropriate electron injection layer (EIL) reduces the electron injection barrier efficiently. Alkali metals and alkali metal halides have been used as a conventional EIL through the n-type doping effect on an electron transport layer (ETL), such as Alq_3 [2,3]. However, alkali metals are not tractable as an evaporation source and are destructively reactive to the organic molecules. On the other hand, alkali metal halides often show variable performance depending upon the cathode choice [4]. Recently, several alternative EILs, such as alkali metal carbonates, nitride and quinolates [5–11] have been studied and show good electron injection performances. Metal oxides such as ZnO, TiO_2 and ZrO_2 are also candidates for alternative EILs [12–14]. Recently, Luo et al. reported highly efficient OLEDs with insulating manganese monoxide (MnO) EIL [15]. However, its detailed working mechanism is not yet understood. Furthermore, the semiconducting phase of metal oxide would be more suitable for device performance than the insulating phase.

In this paper, we propose that semiconducting manganese dioxide (MnO_2) could be a potential candidate as a

* Corresponding author.
E-mail address: yeonjin@yonsei.ac.kr (Y. Yi).

1566-1199/$ - see front matter © 2012 Elsevier B.V. All rights reserved.
doi:10.1016/j.orgel.2012.01.012

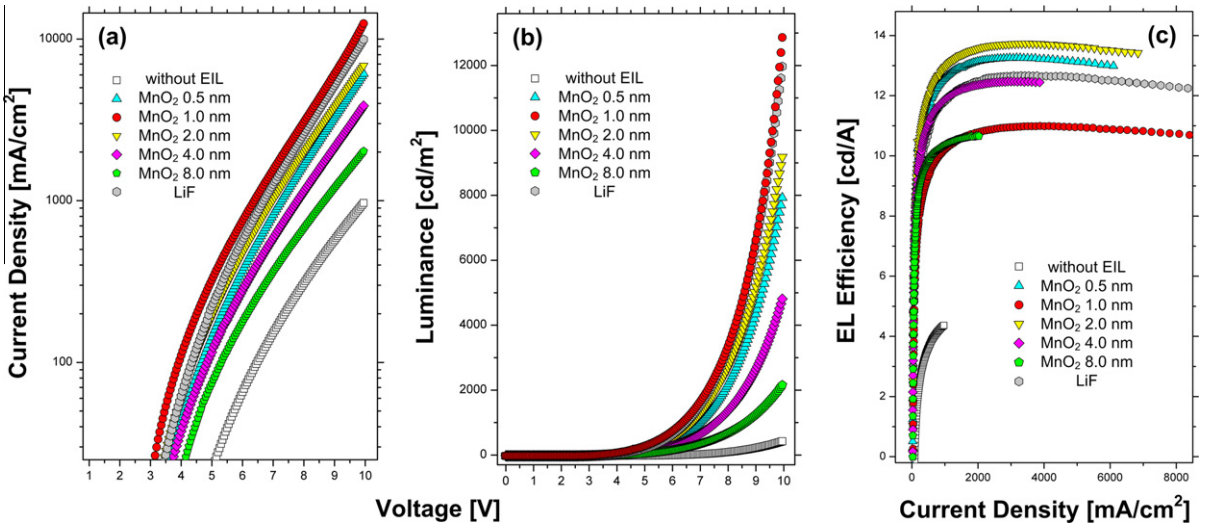

Fig. 1. Measured (a) current density–voltage, (b) luminance–voltage characteristics and (c) EL efficiency of OLEDs with different thicknesses (0, 0.5, 1.0, 2.0, 4.0 and 8.0 nm) of an MnO_2 electron injection layer. The device characteristics with a conventional LiF EIL are also depicted to show the superiority of a MnO_2 EIL.

highly efficient EIL. First, we observed conspicuous enhancements of electron injections with a MnO_2 EIL through OLEDs fabrication including current density–voltage–luminance (*J–V–L*) measurements. We also discovered the optimum thickness of a MnO_2 layer and compared that with a conventional LiF EIL. To elucidate the origin of the electron injection enhancements, we carried out *in situ* photoelectron spectroscopy (PES) experiments. This allowed us to understand the interfacial electronic structures and chemistry which play a crucial role in device performance.

2. Experimental

We fabricated OLEDs with the structure of Al (100 nm)/MnO_2 (0, 0.5, 1.0, 2.0, 4.0, 8.0 nm)/Alq_3 (50 nm)/NPB (50 nm)/ITO. Organic materials and MnO_2 (Sigma Aldrich, 99.99+%) were successively deposited onto the ITO patterned glass substrate by thermal evaporation in an ultra-high vacuum (UHV) chamber below 5×10^{-8} and 2×10^{-7} Torr at the rates of 0.1 nm/s and 0.01 nm/s, respectively. Devices were then completed by depositing the Al cathode on the sample with the rate of >0.1 nm/s. All the deposition rates and thicknesses were monitored by a quartz crystal microbalance. Active areas of the devices are 0.04 cm^2. *J–V–L* characteristics were measured under a dry nitrogen atmosphere using a Keithely 237 and 2400 source measure unit with a photodiode calibrated by a PR650 spectrophotometer. To show the superior electron injection of MnO_2 EIL, OLED with LiF EIL is also fabricated with its optimized thickness (0.1 nm) in our preparation condition.

In situ PES experiments were performed using a PSP RESOLVE 120 spectrometer in an analysis chamber which is directly connected with a preparation chamber. An ultraviolet (He I, 21.22 eV) and a non-monochromatized X-ray (Mg Kα, 1253.6 eV) radiations were used as excitation light sources. To obtain the secondary electron cutoff (SEC), a sample bias of −10 V was applied in normal emission geometry. We used the same interface formation to that of device fabrication because the electronic structures are significantly varied by their deposition sequence between organic and metal electrode [16]. To investigate the effects of the MnO_2 layer insertion, we prepared Al/Alq_3 and Al/MnO_2/Alq_3 samples and compared their electronic structures. In both cases, ITO coated glasses were used as substrates after checking if they all had the same work function. The analysis and preparation chamber were maintained at pressures of 3×10^{-9} and 2×10^{-7} Torr, respectively. The deposition rates were cross checked by a calibrated thickness monitor and by the attenuation of core level intensities in X-ray photoelectron spectroscopy. The interfacial electronic structures of Al/LiF/Alq_3 were referred from well-known reports [4,17].

3. Results and discussion

Fig. 1a and b depicts measured *J–V–L* characteristics. Device performances were highly improved by the insertion of the MnO_2 layer. The optimized thickness of a MnO_2 layer was observed at 1.0 nm and device performance decreased gradually as the MnO_2 layer thickened due to incremental series resistance. However, the device with a relatively thick MnO_2 layer (8.0 nm) still showed better performance than the reference device without MnO_2 insertion. This thickness-independent stability in the device performance originates from the semiconducting nature of MnO_2, which is clear contrast to common EILs such as insulating alkali metal halides [18,19]. As the MnO_2 layer of 1.0 nm is inserted, both current density and luminance increase by more than one order of magnitude at 10 V compared to those of the reference device. Turn on voltage, which is defined as the voltage giving 1 cd/m^2 luminance, was also significantly reduced from 6.4 V to

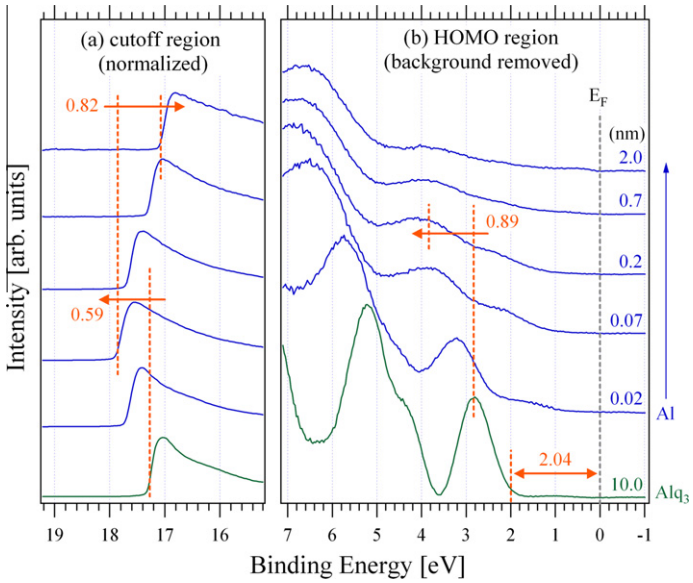

Fig. 2. Measured UPS spectra of (a) the secondary electron cutoff and (b) the HOMO region of Al (0.02, 0.07, 0.2, 0.7 and 2.0 nm)/Alq_3 (10.0 nm). Each spectrum is (a) normalized and (b) background removed for easy comparison, respectively.

3.3 V as the 1.0 nm-MnO_2 was inserted. Furthermore, OLED with 1.0 nm-MnO_2 shows more than 25% higher current density than that of LiF EIL at 10 V. However, as shown in the Fig. 1c, the device with 1.0 nm-MnO_2 interlayer has poorer electroluminescence (EL) efficiency than those with other thicknesses or LiF. Since it clearly shows significant improvement in electron injection from the Al cathode, this low efficiency must be due to the imbalance between electrons and holes within the light emission layer by the excessive electron injection. If one adopted an appropriate hole injection layer too, such as MoO_3 or WO_3 [20,21], EL efficiency could be optimized with an MnO_2 layer of 1.0 nm thickness.

Fig. 2 shows the measured UPS spectra of (a) SEC and (b) the highest occupied molecular orbital (HOMO) region of Al (0.02, 0.07, 0.2, 0.7 and 2.0 nm)/Alq_3 (10.0 nm). The onset of HOMO level of 10.0 nm-Alq_3 is seen at 2.04 eV below the Fermi level. As Al is deposited on Alq_3, SEC shifts to the higher binding energy side until 0.07 nm-Al is deposited. Simultaneously, the HOMO level shifts gradually to the higher binding energy side and the gap state emerges at 2 eV below the Fermi level. As a result, Alq_3 is weakly doped in n-type due to the chemical interaction between Al and Alq_3 without EIL deposition on Alq_3. This interaction has already reported and our results accord well [22]. The total HOMO level shift of Alq_3 is 0.89 eV and the total SEC shift (ΔSEC) is 0.59 eV. After 0.07 nm-Al deposition, SEC shifts to the lower binding energy side, approaching to the work function of Al. Meanwhile, the HOMO level of Alq_3 does not shift any more after 0.2 nm-Al deposition and its intensity is gradually attenuated. Finally, the Fermi level of Al is seen with 2.0 nm-Al deposition.

Fig. 3 displays the measured UPS spectra of (a) SEC and (b) HOMO region of Al (0.02, 0.07, 0.3, 1.0 and 4.0 nm)/MnO_2 (0.5 and 1.0 nm)/Alq_3 (10.0 nm). The onset of HOMO level of 10.0 nm-Alq_3 is seen at 2.06 eV from the Fermi level. As MnO_2 is deposited on Alq_3, the SEC shift to the higher binding energy side is notably larger than that of Al/Alq_3. After 1.0 nm deposition of MnO_2, the SEC shifts by 1.31 eV to the higher binding energy side. Simultaneously, the HOMO level of Alq_3 also shifts by 1.43 eV to the higher binding energy side, which is much larger than that without MnO_2. This implies that the MnO_2 EIL could work efficiently irrespective of the cathode choice unlike LiF/Al vs. LiF/Ag [23,24], where the large HOMO level shift occurs without Al deposition (This will be proven in following device results.) In addition, the amount of HOMO level shift upon the MnO_2 deposition is larger than the reports for Al/LiF/Alq_3, thus it accords well with our device results [4,17,25]. This shift is comparable with that of n-type doping using low work function metals [26]. Furthermore, a broad and weak gap state appears at the high energy position by 1.4 eV apart from the HOMO [inset in (b)]. However, since this gap state becomes visible only after background subtraction and fitting, the interaction between Alq_3 and MnO_2 would be very weak, compared with common interaction features between alkali metals and Alq_3 [27]. Comparing the MnO_2 1.0 nm spectra with that of 0.5 nm, the intensity of the gap state does not noticeably increase. In addition, the valence electronic structure of the pristine Alq_3 is well conserved except for the appearance of a weak gap state upon the MnO_2 deposition. This implies that the n-type doping, electron transfer from MnO_2 to Alq_3, occurs effectively without significant molecular destruction. Ding et al. reported that n-type doping with Cs atoms on organic materials occurred through the following two sequential interactions: (1) the LUMO level shift to the Fermi level at low coverage and (2) the gap state appearance from the LUMO level filling without further energy position shift at high coverage [28,29]. While the interaction (1) reduces the electron injection barrier, the interaction (2) would not contribute to efficient

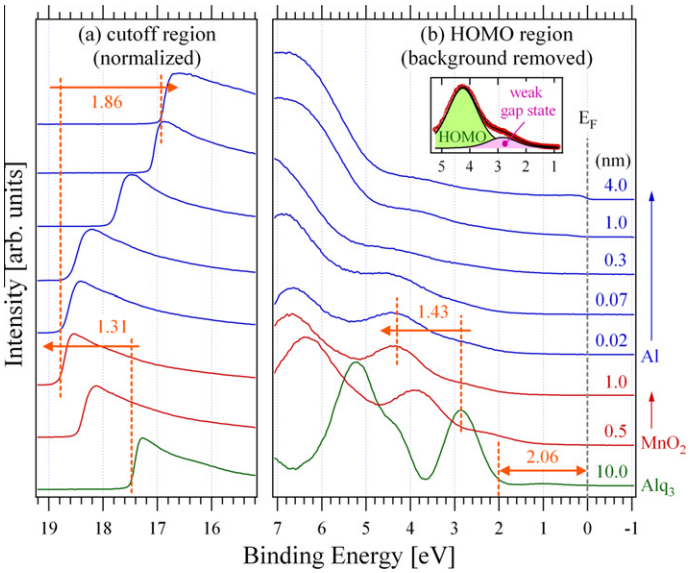

Fig. 3. Measured UPS spectra of (a) the secondary electron cutoff and (b) the HOMO region of Al (0.02, 0.07, 0.3, 1.0 and 4.0 nm)/MnO_2 (0.5 and 1.0 nm)/Alq_3 (10.0 nm). Each spectrum is (a) normalized and (b) background removed for easy comparison, respectively. Magnified HOMO region at MnO_2 1.0 nm is shown in the inset to show the weak broad gap state with peak fitting.

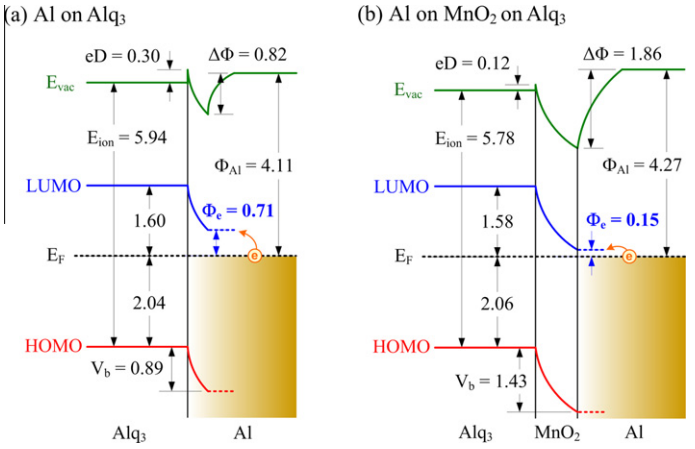

Fig. 4. Energy level diagrams of (a) Al/Alq_3 and (b) Al/MnO_2/Alq_3. Φ_e is the electron injection barrier and E_{ion} is the ionization energy of Alq_3. The band bending (V_b) was evaluated from the shift of the HOMO peak during deposition. Gap states are omitted for brevity.

electron injection anymore and even deteriorates the device performance, because the density of states of the pristine Alq_3 LUMO decreases due to the gap state filling. In general, MnO_2 is known as an n-type semiconductor [30]. Furthermore, thermally evaporated transition metal oxides contain substantial amount of oxygen vacancies, which gives them stronger n-type characteristics [31]. Therefore, Alq_3 could receive electrons from thermally deposited MnO_2 which have enough n-type carriers, i.e. electrons. However, it is expected that the electron transfer from MnO_2 is weaker than that of alkali metals, thus the interaction (1) would be the dominant effect with the MnO_2 EIL. This assumption accords well with the behavior observed in PES spectra where there were large HOMO level shifts indicating significant interaction (1) and a weak gap state indicating insignificant interaction (2). Upon deposition of the Al layer (blue spectra) on the MnO_2 deposited Alq_3, the SEC moves back to lower binding energy side while the HOMO level hardly shifts. The Fermi level of Al is first seen at the Al 1.0 nm deposition step and clearly seen at 4.0 nm. The work function approaches 4.27 eV as the Al layer thickens, which corresponds well with the work function of the Al metal.

Combining all information from the measured spectra, we drew the energy level diagrams of Al/Alq_3 (spectra not shown) and Al/MnO_2/Alq_3 in Fig. 4. The LUMO level of Alq_3 was estimated from the transport band gap of 3.64 eV obtained from the previous report using PES and inverse photoelectron spectroscopy [32]. The ionization energy (E_{ion}) of Alq_3 and the bulk Al work function are both

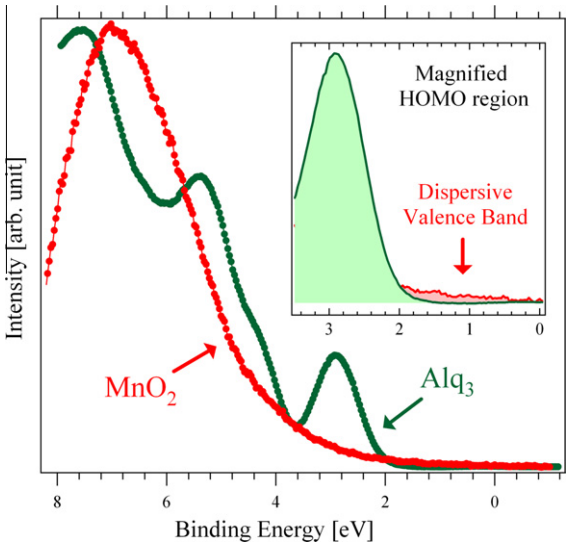

Fig. 5. Measured valence/HOMO region of neat MnO_2 film (5 nm, red mark and line) and Alq_3 film (10 nm, green mark and line) on ITO. To compare them easily, magnified HOMO region is also depicted in the inset. The dispersive valence band of MnO_2 is clearly seen above the HOMO of Alq_3. (For interpretation of the references to color in this figure legend, the reader is referred to the web version of this article.)

within acceptable ranges with regard to the resolution of our system. Band bending (V_b) is determined by the value of the HOMO peak shift and the interfacial dipole (eD) is evaluated by subtracting V_b from ΔSEC. In Fig. 4a, the SEC and HOMO level shift to higher binding energy side upon Al deposition because of the interaction between Al and Alq_3, as shown in PES spectra. Finally, the SEC reaches the work function of Al metal (4.11 eV). As a result, the electron injection barrier (Φ_e) from Al to Alq_3 is measured as 0.71 eV. However, in Fig. 4b, the MnO_2 layer induces a much larger HOMO level shift than the direct Al/Alq_3 interface. No further HOMO shift is observed by subsequent Al deposition, which suggests that the MnO_2 could prevent Al–Alq_3 reactions and would contribute to the device stability. Consequently, Φ_e is dramatically reduced to 0.15 eV, and thus electrons are easily injected from the Al cathode to Alq_3. This is the origin of the electron injection and device performance improvements with a MnO_2 EIL.

To elucidate the origin of the electron transfer from MnO_2 to Alq_3, thus the n-type doping, we measured the valence spectrum of neat MnO_2 thin film and compare it with the HOMO region of Alq_3. We drew the spectra in Fig. 5 with the common vacuum level of neat MnO_2 and Alq_3 film to see the relative level position before the contact formation between MnO_2 and Alq_3. Both spectra were normalized, and backgrounds and He I_β satellites were removed to avoid any confusion. Fig. 5 shows the valence region spectra of MnO_2 (5 nm, red marks and line) and Alq_3 (10 nm, green marks and line) on ITO. While the strong feature of MnO_2 is seen in the range of 5–8 eV, the end tail (emission features at <5 eV) of the dispersive valence band is widely spread over several eVs. This dispersive band is well coincided with the previous XPS and theoretical study [33]. To compare the dispersive valence band of MnO_2 with the HOMO of Alq_3 more clearly, the magnified HOMO region of both spectra are shown in the inset of Fig. 5. The definite dispersive valence band of MnO_2 exists, although its intensity is relatively weak (Generally, in the case of metal oxide film, the end tail of the dispersive energy band is very weak and even it is not observable in PES spectra [34,35].) This density of occupied state could originate from the oxygen vacancies by thermal evaporation, as we aforementioned [31]. The density of occupied state of MnO_2 is broadly distributed far above the HOMO onset of Alq_3 (~2 eV), thus the electrons in this state could easily transfer to the LUMO of Alq_3. This is the origin of the n-type doping properties of MnO_2.

To prove the independence of the cathode choice, we measured the *J–V* characteristics of electron-only devices

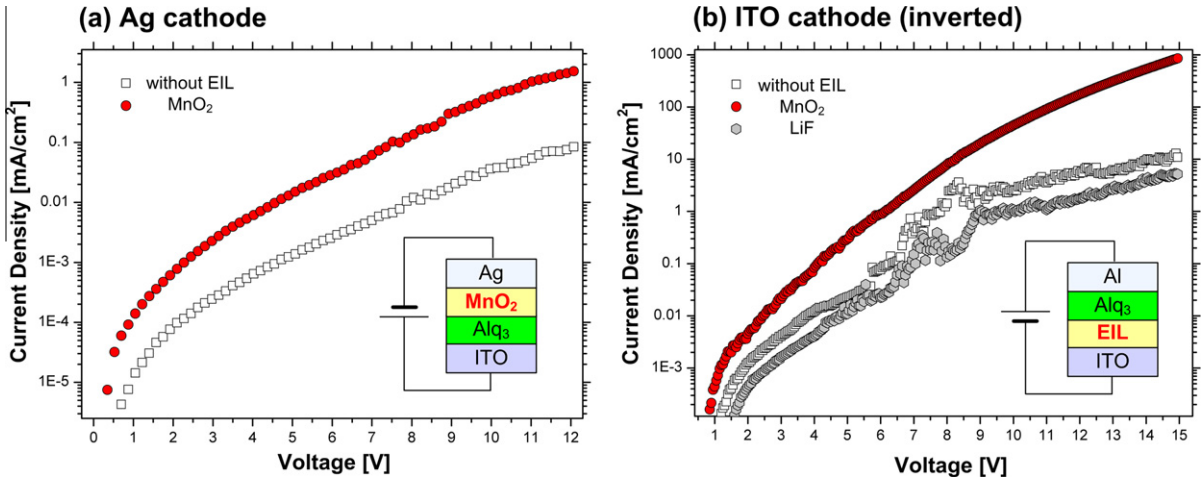

Fig. 6. Measured *J–V* characteristics of electron-only devices with (a) Ag cathode (Ag/MnO_2/Alq_3/ITO) and (b) the inverted structure (Al/Alq_3/EIL/ITO). Schematic configuration of the device is shown in the inset. The MnO_2 devices show much better performance with any cathode–MnO_2 combination than that without EIL.

with two different cathodes in combination with MnO_2 EIL. First, we fabricated the electron-only devices with Ag cathode, which has the device structure of Ag (35 nm)/MnO_2 (1 nm or without)/Alq_3 (300 nm)/ITO. Fig. 6a depicts the measured *J–V* characteristics. At the applied bias of 12 V, MnO_2 device shows higher current density more than one order of magnitude compared to the current density of the device without EIL. This is the identical result, as the *J–V* characteristics of Al/MnO_2 OLEDs, thus MnO_2 EIL works efficiently with Ag cathode, unlike LiF [4,23,24]. In addition, we measured the *J–V* characteristics of the inverted device structures, which consist of Al (100 nm)/Alq_3 (75 nm)/[MnO_2 (1.0 nm)] or [LiF (0.1 nm)] or [without EIL]/ITO. Other conditions are identical as those of our normal OLED structure. In this inverted configuration, ITO was used as a cathode. Measured *J–V* results are shown in Fig. 6b. At 15 V, MnO_2 device shows more than 80 times higher current density than that without EIL. However, LiF EIL does not enhance the *J–V* characteristics at all, even deteriorates, implying that LiF just acts as a resistance. Therefore, MnO_2 is more versatile to be used as an EIL than LiF. In addition, however, we remark the extrinsic factors, such as growth mode of MnO_2 and LiF on ITO, could also highly affect on the *J–V* characteristics.

4. Conclusion

In summary, we investigated significant enhancements of electron injection by inserting the MnO_2 EIL in OLEDs. Device characteristics increase remarkably with MnO_2 EIL and the interfacial electronic structures of Al/Alq_3 and Al/MnO_2/Alq_3 show the prominent reduction of the electron injection barrier from Al to Alq_3, which is comparable or even smaller than that of the conventional EIL, such as LiF or reactive metals. In addition, MnO_2 does not show strong interaction with Alq_3 unlike alkali metals and their halides, which induce molecular distortion/destruction, and instead merely dopes the Alq_3 layer efficiently. The reduction of the electron injection barrier originates from the electron doping effect of MnO_2 having a highly n-type semiconducting nature. Furthermore, efficient electron injection is observed even when MnO_2 is adopted in the device with Ag cathode or inverted structure. These advantages render MnO_2 as a potential alternative for highly efficient EIL.

Acknowledgement

This work was supported by Brain Korea 21 (BK21) project of the ministry of Education, Science and Technology and by a research project of the National Research Foundation of Korea (Grant Nos. 2011-0004748 and 2011-0026100).

References

[1] C.W. Tang, S.A. VanSlyke, Appl. Phys. Lett. 51 (1987) 913.
[2] T. Oyamada, C. Maeda, H. Sasabe, C. Adachi, Jap. J. Appl. Phys. 42 (2003) 1535.
[3] L.S. Hung, C.W. Tang, M.G. Mason, Appl. Phys. Lett. 70 (1997) 152.
[4] C.-I. Wu, G.-R. Lee, T.-W. Pi, Appl. Phys. Lett. 87 (2005) 212108.
[5] C.-I. Wu, C.-T. Lin, Y.-H. Chen, M.-H. Chen, Y.-J. Lu, C.-C. Wu, Appl. Phys. Lett. 88 (2006) 152104.
[6] P.-C. Kao, J.-H. Lin, J.-Y. Wang, C.-H. Yang, S.-H. Chen, Synth. Met. 160 (2010) 1749.
[7] P.-C. Kao, J.-Y. Wang, J.-H. Lin, S.-H. Chen, J. Electrochem. Soc. 157 (2010) J135.
[8] L. Duan, Q. Liu, Y. Li, Y. Gao, G. Zhang, D. Zhang, L. Wang, Y. Qiu, J. Phys. Chem. C 113 (2009) 13386.
[9] K. Xie, J. Qiao, L. Duan, Y. Li, D. Zhang, G. Dong, L. Wang, Y. Qiu, Appl. Phys. Lett. 93 (2008) 183302.
[10] C. Schmitz, H.-W. Schmitz, M. Thelakkat, Chem. Mater. 12 (2000) 3012.
[11] X. Sun, D.-Y. Zhou, L. Qiu, L.-S. Liao, F. Yan, J. Phys. Chem. C 115 (2011) 2433.
[12] H.J. Bolink, E. Coronado, D. Repetto, M. Sessolo, Appl. Phys. Lett. 91 (2007) 223501.
[13] K. Morii, M. Ishida, T. Takashima, T. Shimoda, Q. Wang, M.K. Nazeeruddin, M. Grätzel, Appl. Phys. Lett. 89 (2006) 183510.
[14] N. Tokmoldin, N. Griffiths, D.D.C. Bradley, S.A. Haque, Adv. Mater. 21 (2009) 3475.
[15] J. Luo, L. Xiao, Z. Chen, Q. Gong, Appl. Phys. Lett. 93 (2008) 133301.
[16] Y.M. Lee, Y. Park, Y. Yi, J.W. Kim, Appl. Phys. Lett. 93 (2008) 123301.
[17] Q.T. Le, L. Yan, Y. Gao, M.G. Mason, D.J. Giesen, C.W. Tang, J. Appl. Phys. 87 (2000) 375.
[18] S.J. Kang, D.S. Park, S.Y. Kim, C.N. Whang, K. Jeong, S. Im, Appl. Phys. Lett. 81 (2002) 2581.
[19] K. Han, Y. Yi, W.J. Song, S.W. Cho, P.E. Jeon, H. Lee, C.-N. Whang, K. Jeong, Org. Electron. 9 (2008) 30.
[20] H. You, Y. Dai, Z. Zhang, D. Ma, J. Appl. Phys. 101 (2007) 026105.
[21] J. Meyer, S. Hamwi, T. Bulow, H.-H. Johannes, T. Riedl, W. Kowalsky, Appl. Phys. Lett. 91 (2007) 113506.
[22] L. Yan, M.G. Mason, C.W. Tang, Y. Gao, Appl. Surf. Sci. 175 (2001) 412.
[23] Y.D. Jin, X.B. Ding, J. Reynaert, V.I. Arkhipov, G. Borghs, P.L. Heremans, M.V.d. Auweraer, Org. Electron. 5 (2004) 271.
[24] M. Stöße, J. Staudigel, F. Steuber, J. Blässing, J. Simmerer, A. Winnacker, H. Neuner, D. Metzdorf, H.-H. Johannes, W. Kowalsky, Synth. Met. 111 (2000) 19.
[25] H. Ding, Y. Gao, Appl. Phys. Lett. 91 (2007) 172107.
[26] M.-Y. Chan, S.-L. Lai, K.-M. Lau, M.-K. Fung, C.-S. Lee, S.-T. Lee, Adv. Funct. Mater. 17 (2007) 2509.
[27] N. Johansson, T. Osada, S. Stafstrom, W.R. Salaneck, V. Parente, D.A.d. Santos, X. Crispin, J.-L. Brédas, J. Chem. Phys. 111 (1999) 2157.
[28] H. Ding, Y. Gao, Appl. Phys. Lett. 86 (2005) 213508.
[29] H. Ding, Y. Gao, Appl. Phys. Lett. 92 (2008) 053309.
[30] V.G. Bhide, R.H. Dani, Physica 27 (1961) 821.
[31] C.H. Cheung, W.J. Song, S.K. So, Org. Electron. 11 (2010) 89.
[32] S. Krause, M.B. Case, A. Scholl, E. Umbach, New J. Phys. 10 (2008) 085001.
[33] A.A. Audi, P.M.A. Sherwood, Surf. Interface Anal. 33 (2002) 274.
[34] P. Carreras, S. Gutmann, A. Antony, J. Bertomeu, R. Schlaf, J. Appl. Phys. 110 (2011) 073711.
[35] A. Walsh, J.L.F.D. Silva, S.-H. Wei, C. Körber, A. Klein, L.F.J. Piper, A. DeMasi, K.E. Smith, G. Panaccione, P. Torelli, D.J. Payne, A. Bourlange, R.G. Egdell, Phys. Rev. Lett. 100 (2008) 167402.